Eur. Phys. J. C (2017) 77:817
https://doi.org/10.1140/epjc/s10052-017-5395-3

THE EUROPEAN PHYSICAL JOURNAL C



Regular Article - Theoretical Physics

# Testing holographic conjectures of complexity with Born–Infeld black holes

**Jun Tao**[a], **Peng Wang**[b], **Haitang Yang**[c]

Center for Theoretical Physics, College of Physical Science and Technology, Sichuan University, Chengdu 610064, China

Received: 2 August 2017 / Accepted: 19 November 2017 / Published online: 1 December 2017


**Abstract** In this paper, we use Born–Infeld black holes to test two recent holographic conjectures of complexity, the "Complexity = Action" (CA) duality and "Complexity = Volume 2.0" (CV) duality. The complexity of a boundary state is identified with the action of the Wheeler–deWitt patch in CA duality, while this complexity is identified with the spacetime volume of the WdW patch in CV duality. In particular, we check whether the Born–Infeld black holes violate the generalized Lloyd bound: $\dot{\mathcal{C}} \leq \frac{2}{\pi\hbar}\left[(M-Q\Phi)-(M-Q\Phi)_{\rm gs}\right]$, where gs stands for the ground state for a given electrostatic potential. We find that the ground states are either some extremal black hole or regular spacetime with nonvanishing charges. For Born–Infeld black holes, we compute the action growth rate at the late-time limit and obtain the complexities in CA and CV dualities. Near extremality, the generalized Lloyd bound is violated in both dualities. Near the charged regular spacetime, this bound is satisfied in CV duality but violated in CA duality. When moving away from the ground state on a constant potential curve, the generalized Lloyd bound tends to be saturated from below in CA duality.

## Contents



[a] e-mail: taojun@scu.edu.cn
[b] e-mail: pengw@scu.edu.cn
[c] e-mail: hyanga@scu.edu.cn

## 1 Introduction

Through gauge/gravity duality, concepts from quantum information theory have driven major advances in our understanding of quantum field theory and quantum gravity. For example, the holographic entanglement entropy [1,2] is currently receiving considerable attention in ongoing research. Recently, inspired by the observation that the size of the Einstein–Rosen bridge (ERB) grows linearly at late times, it was conjectured [3–6] that quantum complexity of a boundary state is dual to the volume of the maximal spatial slice crossing the ERB anchored at the boundary state. Roughly speaking, the complexity $\mathcal{C}$ of a state is the minimum number of quantum gates to prepare this state from a reference state [7–9]. However, one of the unappealing features of this proposal is that there is an ambiguity in choosing a length scale in the bulk geometry, which provides some motivations to introduce the "Complexity = Action" (CA) duality [10,11].

In CA duality, the complexity of a boundary state is identified with the action of the Wheeler–deWitt (WdW) patch in the bulk:

$$\mathcal{C} = \frac{S_{\rm WdW}}{\pi\hbar}, \tag{1}$$

where the WdW patch can be defined as the domain of dependence of any Cauchy surface anchored at the boundary state. After the original calculations of $S_{\rm WdW}$ in [11], a detailed analysis was carried out in [12], of the contributions to the action of some subregion from a null segment and a joint at which a null segment is joined to another segment. It is interesting to note that although the two approaches used in [11,12] are different, the results for $\mathrm{d}S_{\rm WdW}/\mathrm{d}t$ at late times of

the AdS Schwarzschild and Reissner–Nordstrom (RN) AdS black holes turn out to be the same. A possible explanation was given in [12].

Similar to the holographic entanglement entropy, the holographic complexity in CA duality is divergent, which is related to the infinite volume near the boundary of AdS space. The divergent terms were considered in [13–15], which showed that these terms could be written as local integrals of boundary geometry. This implies that the divergence comes from the UV degrees of freedom in the field theory. On the other hand, there are two finite quantities associated with the complexity, which can be calculated without first obtaining these divergent terms. The first one is the "complexity of formation" [16], which is the difference of the complexity between a particular black hole and a vacuum AdS spacetime. The second one is the rate of complexity at late times, $\dot{\mathcal{C}}$. If CA duality is correct, $\dot{\mathcal{C}}$ should saturate the Lloyd bound [17]. The Lloyd bound is the conjectured complexity growth bound, which states that $\dot{\mathcal{C}}$ should be bounded by the energy [11]:

$$\dot{\mathcal{C}} \leq \frac{2E}{\pi\hbar}. \tag{2}$$

For a black hole, $E$ is its mass $M$, and the Lloyd bound then reads

$$\dot{\mathcal{C}} \leq \frac{2M}{\pi\hbar}. \tag{3}$$

As noted in [11], the rate of the complexity of a neutral black hole is faster than that of a charged black hole since the existence of conserved charges could put constraints on the system. That implies that the Lloyd bound can be generalized for a charged black hole with the charge $Q$ and potential at the horizon $\Phi$:

$$\dot{\mathcal{C}} \leq \frac{2}{\pi\hbar}\left[(M - Q\Phi) - (M - Q\Phi)_{\rm gs}\right], \tag{4}$$

where $(M - Q\Phi)_{\rm gs}$ is $M - Q\Phi$ calculated in the ground state. A similar bound can also be given for rotating black holes [11]. To distinguish the two bounds given in Eqs. (3) and (4), we shall call the bound in Eq. (3) "the Lloyd bound" and that in Eq. (4) "the generalized Lloyd's bound" in this paper. It showed in [18] that under some general conditions, static vacuum black holes saturated the Lloyd bound in CA duality.

The rate of complexity at the late-time limit in CA duality has been considered in several examples. In [11], it showed that neutral black holes, rotating BTZ black holes, and small RN AdS black holes saturated the corresponding generalized Lloyd bounds, while intermediate and large RN AdS black holes violated the bound (4). Later, it was pointed out [19,20] that even the small RN AdS black holes also violated the generalized bound. The WdW patch action growth of RN AdS black holes, (charged) rotating BTZ black holes, AdS Kerr black holes, and (charged) Gauss–Bonnet black holes were calculated in [19]. The action growth was also discussed in the case of massive gravities [21] and higher derivative gravities [22]. A general case was considered in [23], and it was proved that the action growth rate equals the difference of the generalized enthalpy at the outer and inner horizons. While this paper is in preparation, a preprint [24] appeared, calculating the action growth of Born–Infeld black holes, charged dilaton black holes, and charged black holes with phantom Maxwell field in AdS space. It also showed there that a Born–Infeld AdS black hole with a single horizon and a charged dilaton AdS black hole satisfied the Lloyd bound, while for the charged black hole with a phantom Maxwell field, this bound was violated.

Noting that the thermodynamic volume was related to the linear growth of the WdW patch at late times, Couch *et al.* proposed "Complexity = Volume 2.0" duality in [20]. In "Complexity = Volume 2.0" (CV) duality, the complexity is identified with the spacetime volume of the WdW patch. It was found that the generalized Lloyd bound was violated in both CA and CV dualities for RN AdS black holes near extremality. However, if the ground state was an empty AdS space, this bound was violated in CA duality but satisfied in CV duality. In what follows, let $\mathcal{C}_A/\mathcal{C}_V$ denote the complexity calculated in CA/CV duality.

In this paper, we will check whether the generalized Lloyd bound is violated for the Born–Infeld AdS black holes in CA and CV dualities. The remainder of our paper is organized as follows. In Sect. 2, we discuss some properties of Born–Infeld AdS black holes, which could have a naked singularity, a single horizon, or two horizons depending on their parameters. The phase diagrams for these black holes are obtained. In Sect. 3, we consider the generalized Lloyd bound for the Born–Infeld AdS black holes in CA/CV dualities. In Sect. 4, we conclude with a brief discussion of our results. In the appendix, we employ the approach in [12] to calculate action growth at the late-time limit for $(d+1)$-dimensional Born–Infeld AdS black holes with hyperbolic, planar, and spherical horizons.

## 2 Born–Infeld AdS black holes

In this section, we will consider the black hole solutions of Einstein–Born–Infeld action in $(d+1)$ dimension $(d \geq 3)$ with a negative cosmological constant $\Lambda = -\frac{d(d-1)}{L^2}$. The action of Einstein gravity and the Born–Infeld field reads

$$S = \int_{\mathcal{M}} d^{d+1}x\sqrt{-g}\left(R + \frac{d\,(d-1)}{L^2}\right) + \int_{\mathcal{M}} d^{d+1}x\sqrt{-g}L\,(F)\,, \tag{5}$$

where we take $16\pi G = 1$ for simplicity, $L(F)$ is given by

$$L(F) = 4\beta^2\left(1 - \sqrt{1 + \frac{F^{\mu\nu}F_{\mu\nu}}{2\beta^2}}\right), \tag{6}$$

and $\beta$ is the Born–Infeld parameter. When $\beta \to \infty$, the Lagrangian of Born–Infeld field $L(F)$ becomes that of standard Maxwell field, $L(F) = -F^{\mu\nu}F_{\mu\nu}$. The static black hole solution was obtained in [25,26]:

$$\begin{aligned} ds^2 &= -f(r)\,dt^2 + \frac{dr^2}{f(r)} + r^2 d\Sigma^2_{k,d-1}, \\ F^{rt} &= \frac{\sqrt{(d-1)(d-2)}\beta q}{\sqrt{2\beta^2 r^{2d-2} + (d-1)(d-2)q^2}}, \end{aligned} \tag{7}$$

where

$$\begin{aligned} f(r) = k &- \frac{m}{r^{d-2}} + \left[\frac{4\beta^2}{d(d-1)} + \frac{1}{L^2}\right] r^2 \\ &- \frac{2\sqrt{2}\beta}{d(d-1)r^{d-3}}\sqrt{2\beta^2 r^{2d-2} + (d-1)(d-2)q^2} \\ &+ \frac{2(d-1)q^2}{dr^{2d-4}}\,{}_2F_1\left[\frac{d-2}{2d-2}, \frac{1}{2}, \frac{3d-4}{2d-2}, \right. \\ &\left. - \frac{(d-1)(d-2)q^2}{2\beta^2 r^{2d-2}}\right], \end{aligned} \tag{8}$$

and $d\Sigma^2_{k,d-1}$ is the line element of the $(d-1)$-dimensional hypersurface with constant scalar curvature $(d-1)(d-2)k$ with $k = \{-1, 0, 1\}$. Note that the black holes with $k = \{-1, 0, 1\}$ have hyperbolic, planar, and spherical horizons. The mass $M$ and charge $Q$ of the Born–Infeld black hole are given by, respectively,

$$\begin{aligned} M &= (d-1)\Omega_{k,d-1}m, \\ Q &= \frac{\sqrt{(d-1)(d-2)}\Omega_{k,d-1}}{4\pi\sqrt{2}}q, \end{aligned} \tag{9}$$

where $\Omega_{k,d-1}$ denotes the dimensionless volume of $d\Sigma^2_{k,d-1}$. For $k = 0$ and $-1$, one needs to introduce an infrared regulator to produce a finite value of $\Omega_{k,d-1}$.

For the sake of calculating the action growth and thermodynamic volume of the Born–Infeld black holes, we need to determine the number of their horizons. Depending on the values of the parameters $q$ and $m$, the black holes could possess a naked singularity at $r = 0$, one, or two horizons. In fact, we could define a $q$-dependent function

$$b(r, q) = r^{d-2} f(r) + m, \tag{10}$$

which does not depend on the parameter $m$. For a given value of $m$, one could solve $b(r, q) = m$ for the position of the horizon. The derivative of $b(r, q)$ with respect to $r$ is

$$\begin{aligned} \frac{db(r,q)}{dr} = (d-2)r^{d-3}\Bigg[k + \frac{dr^2}{(d-2)L^2} \\ - \frac{2q^2}{r^{d-3}\left(r^{d-1} + \sqrt{r^{2d-2} + \frac{(d-1)(d-2)q^2}{2\beta^2}}\right)}\Bigg], \end{aligned} \tag{11}$$

which is a strictly increasing function. When $r \to \infty$, $db(r, q)/dr$ goes to $\infty$. In the limit $r \to 0$, we find that

$$\begin{aligned} \frac{db(r,q)}{dr}|_{r=0} &= -\frac{2\sqrt{2}\beta q}{(d-1)}\sqrt{(d-1)(d-2)}, \text{ for } d > 3, \\ \frac{db(r,q)}{dr}|_{r=0} &= k - 2\beta q, \text{ for } d = 3, \end{aligned} \tag{12}$$

which shows that $db(r, q)/dr|_{r=0} \geq 0$ in the $k = 1$, $d = 3$, and $\beta q \leq 1/2$ case, and $db(r, q)/dr|_{r=0} < 0$ in the other cases. When $\frac{db(r,q)}{dr}|_{r=0} < 0$, the equation $db(r, q)/dr = 0$ has one and only solution $r_e(q) > 0$, such that $db(r, q)/dr|_{r=r_e(q)} = 0$. Thus, there is an extremal black hole solution with the parameter $m = b(r_e(q), q)$ and the horizon being at $r = r_e(q)$. At $r = r_e(q)$, we obtain

$$\begin{aligned} b(r_e(q), q) = \frac{2}{d}kr_e^{d-2} + \frac{2(d-1)q^2}{dr_e^{d-2}} \\ \times {}_2F_1\left[\frac{d-2}{2d-2}, \frac{1}{2}, \frac{3d-4}{2d-2}, -\frac{(d-1)(d-2)q^2}{2\beta^2 r_e^{2d-2}}\right]. \end{aligned} \tag{13}$$

When $k = 0$ and $1$, $b(r_e(q), q)$ is always positive. However, for $k = -1$, $b(r_e(q), q)$ could be negative for some values of $q$. It is noteworthy that $b(r_e(q), q)$ exists for $q \geq \frac{1}{2\beta}$ in the $k = 1$, $d = 3$, and $\beta q \leq 1/2$ case, while $b(r_e(q), q)$ exists for all values of $q$ in other cases. Moreover, one finds that

$$b(0, q) = A(q) > 0, \tag{14}$$

where

$$\begin{aligned} A(q) \equiv \frac{2(d-1)q^2}{d}\frac{\Gamma\left(\frac{3d-4}{2d-2}\right)\Gamma\left(\frac{1}{2(d-1)}\right)}{\sqrt{\pi}} \\ \times \left[\frac{2\beta^2}{(d-1)(d-2)q^2}\right]^{\frac{d-2}{2(d-1)}}. \end{aligned} \tag{15}$$

Since $db(r, q)/dr < 0$ for $0 < r < r_e$, one obtains $b(r_e(q), q) < b(0, q) = A(q)$. In Fig. 1, we plot the function $b(r, q)$ against $r$ for different values of $q$, where we take $L = 1$ and $\beta = 10$.

With the above results, we can discuss when the Born–Infeld black hole solution (7) possesses a naked singularity, a single horizon, or two horizons:

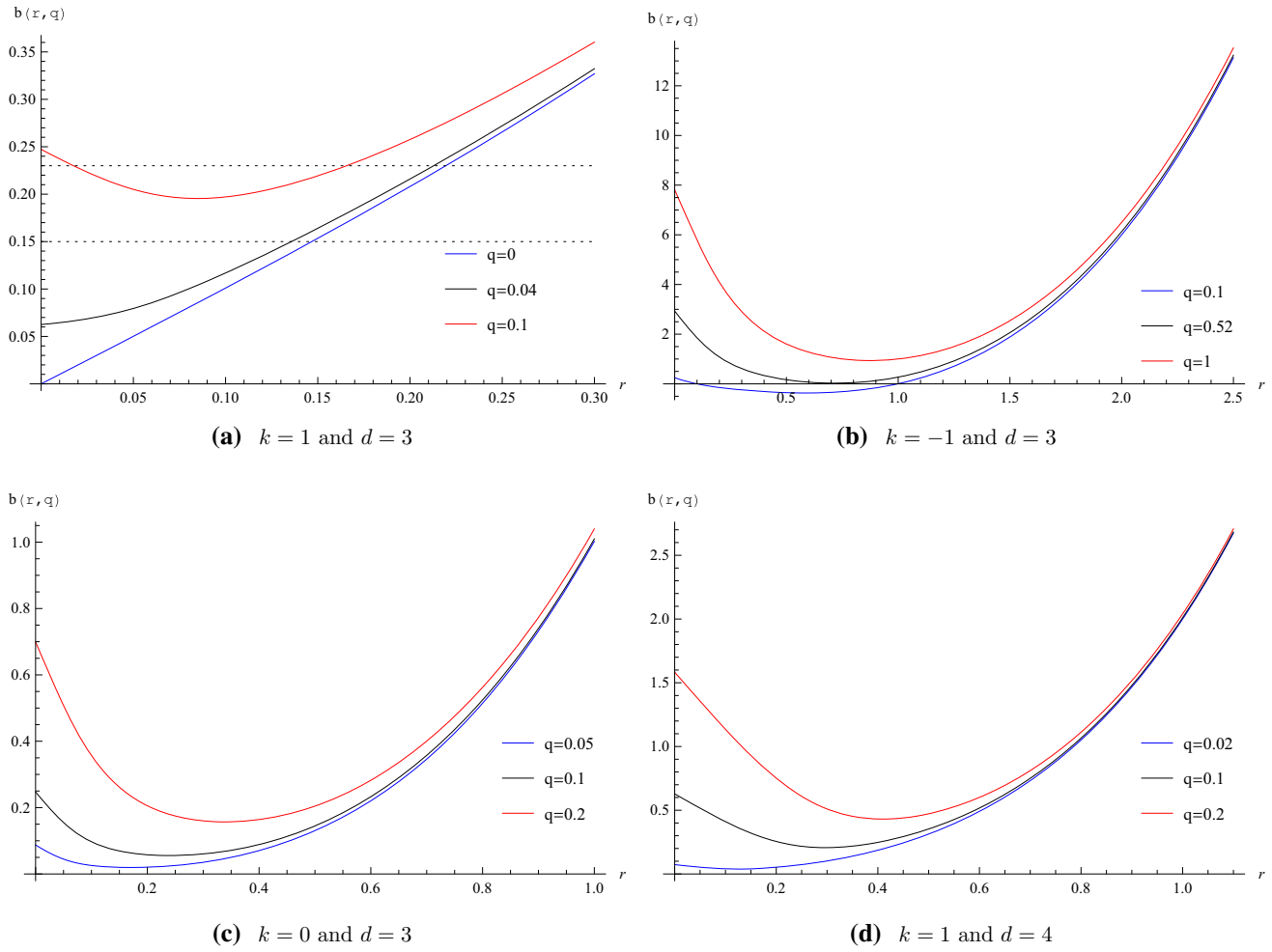


**(a)** $k = 1$ and $d = 3$ **(b)** $k = -1$ and $d = 3$

**(c)** $k = 0$ and $d = 3$ **(d)** $k = 1$ and $d = 4$

**Fig. 1** Plots of $b\,(r, q)$ versus $r$ for different values of $q$, where $L = 1$ and $\beta = 10$

- Single Horizon: $m \geq A\,(q)$. For example, $\{q = 0.04, m = 0.15\}$ in Fig. 1a.
- Two Horizons: $b\,(r_e\,(q)\,, q) \leq m < A\,(q)$. For example, $\{q = 0.1, m = 0.23\}$ in Fig. 1a.
- Naked Singularity: $m < A\,(q)$ when $k = 1$, $d = 3$, and $\beta q \leq 1/2$; $m < b\,(r_e\,(q)\,, q)$ in the other cases. For example, $\{q = 0.1, m = 0.15\}$ in Fig. 1a.

The phase diagrams for Born–Infeld AdS black holes are plotted in Fig. 2, for the cases with $\{d = 3, k = \pm 1, 0\}$ and $\{d = 4, k = 1\}$. We also take $L = 1$ and $\beta = 10$ in Fig. 2. The blue lines in Fig. 2 are extremal lines, which are given by $m = b\,(r_e\,(q)\,, q)$. The boundaries between the black holes with one horizon and these with two horizons are depicted as the black dashed lines, which are given by $m = A\,(q)$. The colored lines (red and blue) are the boundaries between black holes and naked singularities. In Fig. 2a, the red line divides the black holes with a single horizon and the spacetime with a naked singularity, and it meets the blue extremal line at the red dot, whose $q$ coordinate is $\frac{1}{2\beta} = 0.05$.

To discuss the generalized Lloyd bounds, we need to specify the electrostatic potential of the ground states, which are the colored lines in the inset subfigures of Fig. 2. The electrostatic potential at the black hole horizon, which is conjugate to the electric charge $Q$, is [25,26]

$$\Phi = \sqrt{\frac{d-1}{2\,(d-2)}}\frac{16\pi q}{r_h^{d-2}}\,{}_2F_1\left[\frac{d-2}{2d-2}, \frac{1}{2}, \frac{3d-4}{2d-2}, -\frac{(d-1)\,(d-2)\,q^2}{2\beta^2 r_h^{2d-2}}\right], \tag{16}$$

where $r_h$ is the horizon's radius. The blue lines in the inset subfigures of Fig. 2 are the potential of the extremal black holes, which are obtained by plugging the extremal radius $r_e\,(q)$ into Eq. (16). In Fig. 2a, the black holes on the red line possess a single horizon, whose radius $r_h$ is zero. The red line in the inset subfigure of Fig. 2a is the potential of these black holes, which is the limit value of Eq. (16) at

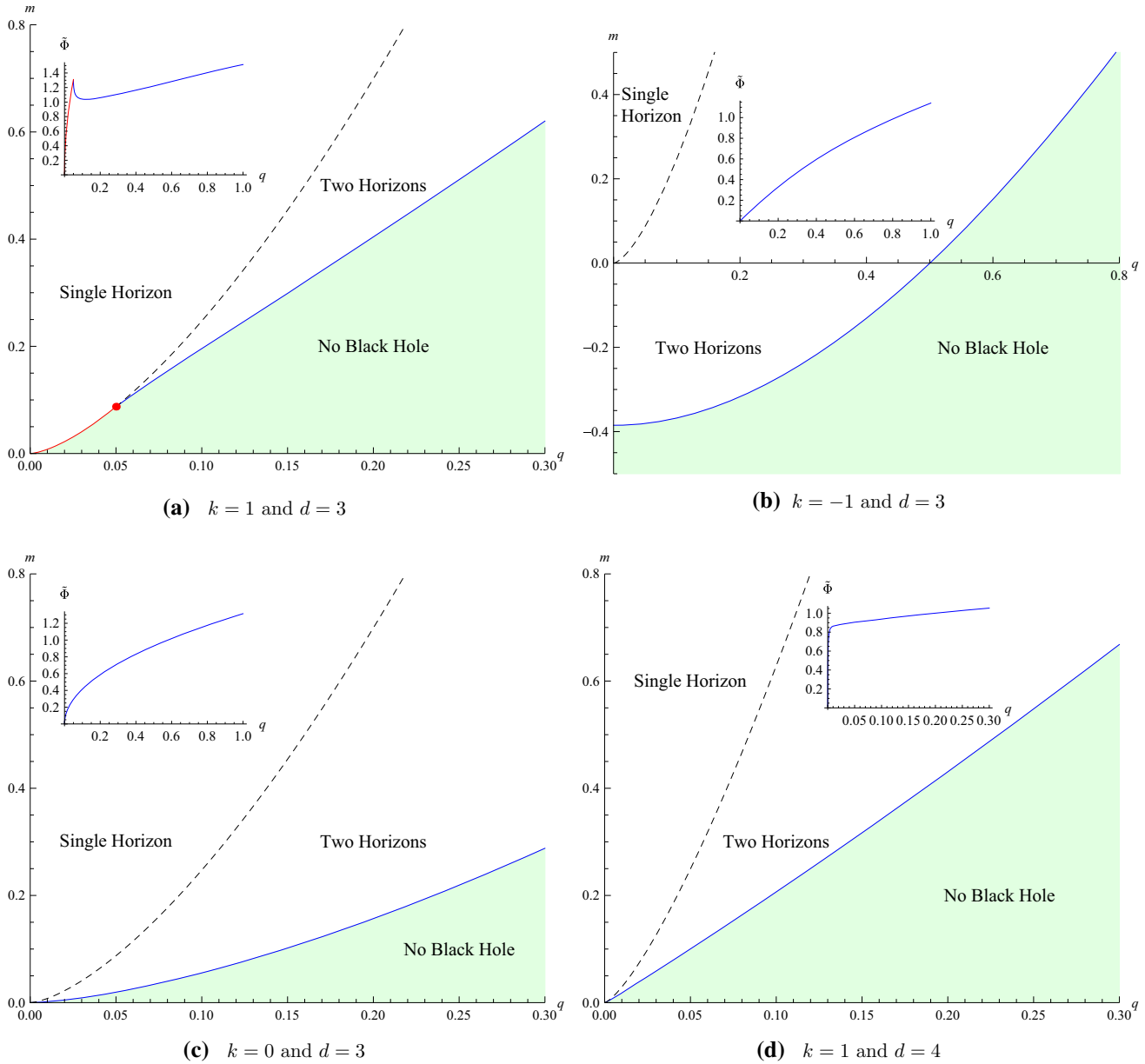


**(a)** $k = 1$ and $d = 3$ **(b)** $k = -1$ and $d = 3$

**(c)** $k = 0$ and $d = 3$ **(d)** $k = 1$ and $d = 4$

**Fig. 2** The phase diagrams for Born–Infeld AdS black holes where $L = 1$ and $\beta = 10$. The blue lines are extremal black holes, while the red one is some regular spacetime with nonvanishing charges. Small figures are the plots of the potential along the boundary lines

$r_h = 0$. When $\beta \to \infty$, the Born–Infeld AdS black holes become the RN AdS black holes. When $k = 1$ and $d = 3$, it was found [11] that the boundary of RN AdS black holes in the phase diagram was the extremal line, and the potential $\Phi$ approached $16\pi$ as $(q, m) \to (0, 0)$ along the extremal line. Thus, for a RN AdS black hole, the ground state of the geometry with the same electrostatic potential as this black hole is pure AdS spacetime for $\frac{\Phi}{16\pi} \leq 1$, but for $\frac{\Phi}{16\pi} > 1$ it is some extremal black hole. Now we compute the asymptotic behavior of $\Phi$ as $(q, m) \to (0, 0)$ along the boundaries:

- $k = 0$: The boundary is the extremal line, on which $r_e \sim q^{\frac{1}{d-1}}$ given by $\mathrm{d}b\,(r, q)\,/\mathrm{d}r|_{r=r_e} = 0$. Since $\frac{q^2}{r_e^{2d-2}} \sim 1$ as $q \to 0$, we find

$$\Phi \sim \frac{q}{r_e^{d-2}} \sim q^{\frac{1}{d-1}} \to 0 \quad \text{as } q \to 0. \tag{17}$$

- $k = -1$: The boundary is the extremal line, on which $r_e \sim L$ as $q \to 0$. One then finds

$$\Phi \sim \frac{q}{r_e^{d-2}} \sim q \to 0 \quad \text{as } q \to 0. \tag{18}$$

It is interesting to note that

$$m \to \frac{2}{d}\left(\frac{d-2}{d}\right)^{\frac{d-2}{2}} L^{d-2} \quad \text{as } q \to 0. \tag{19}$$

- $k = 1$: If $d > 3$, the extremal line could go to $(0, 0)$ as $q \to 0$. On the extremal line, $\mathrm{d}b\,(r, q)\,/\mathrm{d}r|_{r=r_e} = 0$ shows that $r_e \sim q^{\frac{1}{d-3}}$ and $\frac{q^2}{r_e^{2d-2}} \to \infty$ as $q \to 0$. Using Eq. (16), we also find

$$\Phi \sim q^{\frac{1}{d-1}} \to 0. \tag{20}$$

If $d = 3$, the boundary line around $(0, 0)$ is the red line in Fig. 2a, on which $r_+ = 0$. Again, we have

$$\Phi \propto q^{\frac{1}{d-1}} \to 0. \tag{21}$$

Unlike the $k = 1$ and $d = 3$ RN AdS black holes, the potential $\Phi \to 0$ as $(q, m) \to (0, 0)$ along the boundary lines for the Born–Infeld AdS black holes. Thus, for a Born–Infeld AdS black hole with $\Phi > 0$, the ground state of the geometry with the same $\Phi$ is either some extremal black hole (blue lines) or some regular spacetime with nonvanishing charges (red lines). In the cases with $\{d = 3, k = \pm 1, 0\}$ and $\{d = 4, k = 1\}$, the potential along the boundary lines are plotted in Fig. 2, where $\tilde{\Phi} = \frac{\Phi}{16\pi}$, $L = 1$, and $\beta = 10$.

## 3 Holographic conjectures of complexity

In this section, we will discuss CA/CV dualities for the Born–Infeld AdS black holes. In our appendix, the action growth of the Born–Infeld AdS black holes within the WdW patch at late-time approximation is calculated by following the approach in [12]. The action growth at the late-time limit in the case with $k = 1$ and $d = 3$ was first calculated in [19]. The growth rate of the action $\mathrm{d}S/\mathrm{d}t$ depends on the number of the horizons. In fact, we find that

$$\begin{aligned}\frac{\mathrm{d}S}{\mathrm{d}t} &= 2M - Q\Phi_+ - (d-2)\,A\,(q)\,\Omega_{k,d-1} \\ &\quad \text{in the case of one horizon,} \\ \frac{\mathrm{d}S}{\mathrm{d}t} &= Q\Phi_- - Q\Phi_+ \text{ in the case of two horizons,}\end{aligned} \tag{22}$$

where $\Phi$ is the potential at the horizon given by Eq. (16), $\Phi_\pm$ are $\Phi$ calculated at $r = r_\pm$, and $r_\pm$ is the radius of the $\substack{\text{outer}\\\text{inner}}$ horizon. Furthermore, CA duality indicates that, in the late-time regime,

$$\dot{\mathcal{C}}_A = \frac{1}{\pi\hbar}\frac{\mathrm{d}S}{\mathrm{d}t}. \tag{23}$$

On the other hand, CV duality gives [20] that, in the late-time regime,

$$\dot{\mathcal{C}}_V = \frac{PV}{\hbar}, \tag{24}$$

where $P = d\,(d-1)\,/L^2$ is the pressure, and $V$ is the volume of the WdW patch. For Born–Infeld AdS black holes, the rate of the complexity at late times is then given by

$$\begin{aligned}\dot{\mathcal{C}}_V &= \frac{(d-1)\,\Omega_{k,d-1} r_+^d}{L^2\hbar} \text{ in the case of one horizon,} \\ \dot{\mathcal{C}}_V &= \frac{(d-1)\,\Omega_{k,d-1}\left(r_+^d - r_-^d\right)}{L^2\hbar} \text{ in the case of two horizons.}\end{aligned} \tag{25}$$

The generalized Lloyd bound for a charged black hole is

$$\dot{\mathcal{C}} \le \frac{2}{\pi\hbar}\left[(M - Q\Phi) - (M - Q\Phi)_{\mathrm{gs}}\right], \tag{26}$$

where $(M - Q\Phi)_{\mathrm{gs}}$ is $M - Q\Phi$ calculated in the ground state. The ground state is on the boundary between black hole region and no black hole region (colored lines in Fig. 2). If the system is treated as a grand canonical ensemble, the ground state has the same potential $\Phi$ as the black hole under consideration. Now we will calculate the rate of the complexity in the CA and CV dualities and check whether the generalized Lloyd bound (26) is violated.

### 3.1 A. Around extremal line

We first consider a general static charged black hole with the line element

$$\mathrm{d}s^2 = -f\,(r)\,\mathrm{d}t^2 + \frac{\mathrm{d}r^2}{f\,(r)} + r^2\mathrm{d}\Sigma_{k,d-1}^2, \tag{27}$$

where the radii of the outer and inner horizon are $r_+$ and $r_-$, respectively. The first law of black hole thermodynamics reads

$$\mathrm{d}M = T\mathrm{d}S + \Phi\mathrm{d}Q. \tag{28}$$

Since the entropy $S$ is a function of $r_+$, one finds

$$\begin{aligned}\frac{\partial M\,(r_+, Q)}{\partial Q} &= \Phi, \\ \frac{\partial M\,(r_+, Q)}{\partial r_+} &= T\frac{\mathrm{d}S}{\mathrm{d}r_+}.\end{aligned} \tag{29}$$

At extremality where $T = 0$, we have

$$\frac{\partial M\,(r_+, Q_e)}{\partial r_+}|_{r_+=r_e} = 0, \tag{30}$$

where $r_e$ and $Q_e$ are the radius and charge, respectively, of the black hole at extremality. For a fixed value of $\Phi$, $r_+$ can be determined by $Q : r_+ = r_+ (Q)$. Thus on the constant $\Phi$ curve near extremality, we find

$$\begin{aligned} & M\left(r_+\left(Q_e+\delta Q\right), Q_e+\delta Q\right)-\left(Q_e+\delta Q\right)\Phi \\ & \quad -\left[M\left(r_+\left(Q_e\right), Q_e\right)-Q_e\Phi\right] \\ & \quad =\left[\left(\frac{\partial M\left(r_+, Q\right)}{\partial r_+}\frac{\mathrm{d}r_+(Q)}{\mathrm{d}Q}\right)|_{Q=Q_e}\delta Q\right. \\ & \qquad \left.+\frac{\partial M\left(r_+, Q\right)}{\partial Q}|_{Q=Q_e}\delta Q-\Phi\delta Q\right] \\ & \qquad +\mathcal{O}\left(\delta Q^2\right)\sim\mathcal{O}\left(\delta Q^2\right). \end{aligned} \tag{31}$$

The generalized Lloyd bound then becomes

$$\frac{2}{\pi\hbar}\left[(M-Q\Phi)-(M-Q\Phi)_{\mathrm{gs}}\right]\sim\mathcal{O}\left(\delta Q^2\right). \tag{32}$$

Expanding $r_\pm$ near extremality, we find that

$$r_\pm\approx r_e+c_1^\pm\delta Q, \tag{33}$$

where

$$\begin{aligned} c_1^+ &= -\frac{\partial_Q\Phi\left(r_e, Q_e\right)}{\partial_{r_+}\Phi\left(r_e, Q_e\right)}, \\ c_1^- &= \frac{\partial_Q\Phi\left(r_e, Q_e\right)}{\partial_{r_+}\Phi\left(r_e, Q_e\right)}-\frac{2\partial_r\Phi\left(r_e, Q_e\right)}{\partial_{r_+}^2 M\left(r_e, Q_e\right)}. \end{aligned} \tag{34}$$

From these results we can expand $\dot{\mathcal{C}}$ near extremality as

$$\begin{aligned} \dot{\mathcal{C}}_A &\sim \frac{Q_e\partial_{r_+}\Phi\left(r_e, Q_e\right)}{\pi\hbar}\left(c_1^+-c_1^-\right)\delta Q, \\ \dot{\mathcal{C}}_V &\sim \frac{d\left(d-1\right)\Omega_{k,d-1}r_e^{d-1}}{L^2\hbar}\left(c_1^+-c_1^-\right)\delta Q. \end{aligned} \tag{35}$$

If $c_1^+\neq c_1^-$, the generalized Lloyd bounds are violated near extremality under the two proposals. For the Born–Infeld AdS black holes with $d=3$, we find that

$$\begin{aligned} c_1^+-c_1^- = & \frac{k-\tilde{\Phi}^2}{\tilde{\Phi}^2\left(k-2\tilde{\Phi}^2\right)} \\ & -\frac{3\left(k^2-8k\tilde{\Phi}^2+6\tilde{\Phi}^4\right)}{10\beta^2L^2\left(k-2\tilde{\Phi}^2\right)^2\left(k-\tilde{\Phi}^2\right)}+\mathcal{O}\left(\beta^{-4}\right), \end{aligned} \tag{36}$$

where $\tilde{\Phi}=\frac{\Phi}{16\pi}$.

### 3.2 B. Around regular charged spacetime

Shown in Fig. 2a is a red boundary, which is $m=A\left(q\right)$ for $q\leq\frac{1}{2\beta}$, in the case with $d=3$ and $k=1$. Above this boundary, one has a black hole with a single horizon, whose radius goes to zero on approaching the boundary. When $r\ll 1$, we find

$$f\left(r\right)=\left(1-2q\beta\right)-\frac{m-A\left(q\right)}{r}+\mathcal{O}\left(r^2\right), \tag{37}$$

which means that the metric is regular at $r=0$ for $m=A\left(q\right)$. Therefore, one has some regular spacetime with nonvanishing charges on the red boundary. The potential $\Phi\left(=16\pi\tilde{\Phi}\right)$ of the ground states on the boundary can be obtained from finding the limit of Eq. (16) as $r_+\to 0$:

$$\tilde{\Phi}=\tilde{\Phi}_c\sqrt{2q\beta}\leq\tilde{\Phi}_c, \tag{38}$$

where

$$\tilde{\Phi}_c=\frac{1}{\sqrt{2\pi}}\Gamma\left(\frac{5}{4}\right)\Gamma\left(\frac{1}{4}\right). \tag{39}$$

A little bit above the boundary, the radius of a black hole with the potential $\Phi$ is given by

$$r_+\approx\frac{\tilde{\Phi}_c^2}{\tilde{\Phi}^2+\tilde{\Phi}_c^2}\delta m, \tag{40}$$

where $\delta m=m-m_0$, and $m_0$ is the $m$ parameter of the ground state with the same potential $\Phi$. Since $r_+\ll 1$ implied by Eq. (40), Eq. (37) shows that the temperature of the black hole is

$$T\propto m-A\left(q\right), \tag{41}$$

which goes to zero on approaching the ground state. For this black hole, we find that the generalized Lloyd bound is

$$\begin{aligned} & \frac{2}{\pi\hbar}\left[(M-Q\Phi)-(M-Q\Phi)_{\mathrm{gs}}\right] \\ & \quad\approx\frac{16}{\hbar}\left(1-\frac{2\tilde{\Phi}^2}{\tilde{\Phi}^2+\tilde{\Phi}_c^2}\right)\delta m. \end{aligned} \tag{42}$$

On the other hand, we can expand $\dot{\mathcal{C}}$ as

$$\begin{aligned} \dot{\mathcal{C}}_A &\approx \frac{16}{\hbar}\left(1-\frac{3}{2}\frac{\tilde{\Phi}^2}{\tilde{\Phi}^2+\tilde{\Phi}_c^2}\right)\delta m, \\ \dot{\mathcal{C}}_V &\sim \mathcal{O}\left(r_+^3\right)\sim\mathcal{O}\left(\delta m^3\right). \end{aligned} \tag{43}$$

It appears that the bound is satisfied in CV duality although far from saturated near the boundary. However, the bound is violated in CA duality.

### 3.3 C. Large $q$ on constant $\Phi$ curve

Consider Born–Infeld AdS black holes with fixed potential $\Phi$. When $q \to \infty$ along the constant $\Phi$ curve, one could have there possibilities for $\frac{q^2}{r_+^{2d-2}}$: $\frac{q^2}{r_+^{2d-2}} \to 0$, $\frac{q^2}{r_+^{2d-2}} \to C$ where $0 < C < \infty$, and $\frac{q^2}{r_+^{2d-2}} \to \infty$. If $\frac{q^2}{r_+^{2d-2}} \to \infty$, Eq. (16) gives that $\Phi \sim q^{\frac{1}{d-1}}$, which cannot be a constant. Similarly for $\frac{q^2}{r_+^{2d-2}} \to C$, one has that $\Phi \sim r_+ \sim q^{\frac{1}{d-1}}$. Therefore, we could only have

$$\frac{q^2}{r_+^{2d-2}} \to 0 \quad \text{as } q \to \infty \text{ along the constant } \Phi \text{ curve.} \tag{44}$$

Expanding Eq. (16) in terms of $\frac{q}{r_+^{d-1}}$ and solving for $q$, one has

$$q \sim \sqrt{\frac{2\,(d-2)}{d-1}}\tilde{\Phi} r_+^{d-2}\left(1+\frac{(d-2)^3}{2\,(3d-4)}\frac{\tilde{\Phi}^2}{\beta^2 r_+^2}\right). \tag{45}$$

Since Eq. (44) implies that $r_+ \gg 1$ when $q \gg 1$, the parameter $m$ is

$$m = \frac{r_+^d}{L^2}\left[1+\mathcal{O}\left(r_+^{-2}\right)\right]. \tag{46}$$

The generalized Lloyd bound for $q \gg 1$ ($r_+ \gg 1$) is then given by

$$\begin{aligned}&\frac{2}{\pi\hbar}\left[(M-Q\Phi)-(M-Q\Phi)_{\rm gs}\right]\\ &=\frac{2\,(d-1)\,\Omega_{k,d-1}}{\pi\hbar}\frac{r_+^d}{L^2}\left[1+\mathcal{O}\left(r_+^{-2}\right)\right].\end{aligned} \tag{47}$$

From Eqs. (45) and (46), it follows that

$$m \sim q^{\frac{d}{d-2}} \text{ for } q \gg 1. \tag{48}$$

Since $A\,(q) \sim q^{\frac{d}{d-1}}$, the Born–Infeld AdS black holes with fixed potential $\Phi$ always lie above the $m = A\,(q)$ line for large enough $q$, which means that these black holes always possess a single horizon for $q \gg 1$ with fixed $\Phi$. Therefore, Eqs. (22) and (25) give

$$\begin{aligned}\dot{\mathcal{C}}_A &= \frac{2\,(d-1)\,\Omega_{k,d-1}}{\pi\hbar}\frac{r_+^d}{L^2}\left[1-\frac{C_d L^2\tilde{\Phi}^{\frac{d}{d-1}}\beta^{\frac{d-2}{d-1}}}{2\,(d-1)\,\Omega_{k,d-1}}r_+^{\frac{-d}{d-1}}\right.\\ &\quad\left.+\mathcal{O}\left(r_+^{-2}\right)\right],\\ \dot{\mathcal{C}}_V &= \frac{(d-1)\,\Omega_{k,d-1}r_+^d}{L^2\hbar},\end{aligned} \tag{49}$$

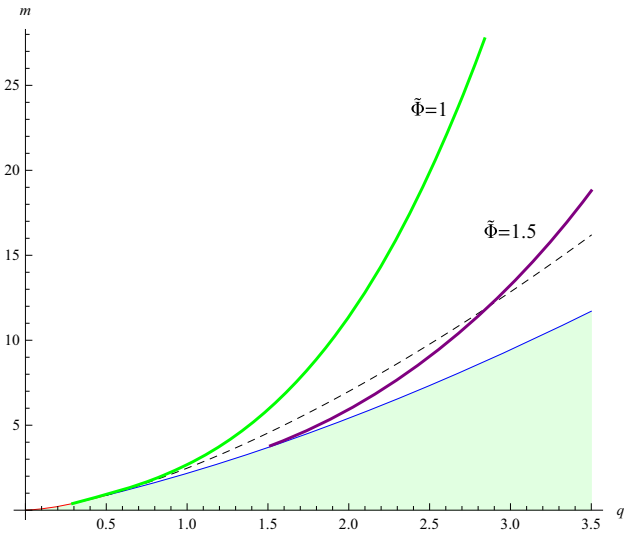


**Fig. 3** Curves of constant potential $\tilde{\Phi} = 1$ and 1.5 in the case with $d = 3$, $k = 1$, $L = 1$ and $\beta = 1$

where

$$\begin{aligned}C_d &= \frac{2\,(d-1)}{d}\frac{\Gamma\left(\frac{3d-4}{2d-2}\right)\Gamma\left(\frac{1}{2(d-1)}\right)}{\sqrt{\pi}}\\ &\quad\times\left(\frac{2}{d-1}\right)^{\frac{d-2}{d-1}}\left[\frac{2\,(d-2)}{d-1}\right]^{\frac{1}{d-1}}.\end{aligned} \tag{50}$$

We see immediately that the generalized Lloyd bound is satisfied in CA duality for sufficiently large $q$ and tends to be saturated as $q \to \infty$. However, in CV duality, $\dot{\mathcal{C}}$ is $\pi/2$ times as large as the generalized Lloyd bound for $q \gg 1$.

### 3.4 D. Numerical results

Here we consider two curves of constant potential, $\tilde{\Phi} = 1$ and $\tilde{\Phi} = 1.5$, in the case with $d = 3$ and $k = 1$. These two constant potential curves are plotted in Fig. 3 for $\beta = 1$. Note that the $\tilde{\Phi} = 1$ curve (green) starts from some regular spacetime, while the $\tilde{\Phi} = 1.5$ curve (purple) starts from some extremal black hole. Both curves enter the "Single Horizon" region for large enough $q$, which is in agreement with the argument below Eq. (48).

To check whether the generalized Lloyd bound is violated on the curves, we define

$$\begin{aligned}R_A &= \frac{\dot{\mathcal{C}}_A}{\frac{2}{\pi\hbar}\left[(M-Q\Phi)-(M-Q\Phi)_{\rm gs}\right]},\\ R_V &= \frac{\dot{\mathcal{C}}_V}{\frac{2}{\pi\hbar}\left[(M-Q\Phi)-(M-Q\Phi)_{\rm gs}\right]}.\end{aligned} \tag{51}$$

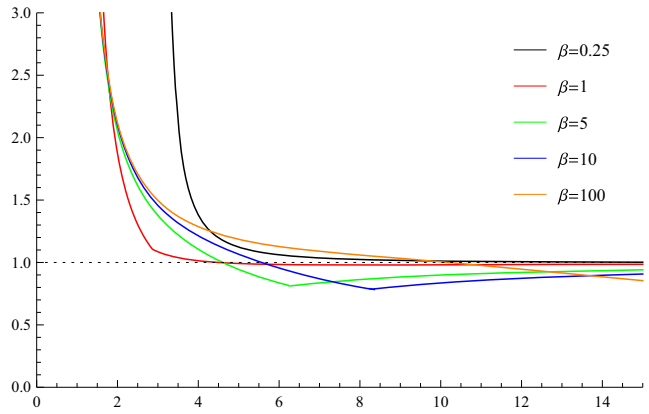


**(a)** Plot of $R_A$ versus $q$ in CA-duality along the $\tilde{\Phi} = 1.5$ curve starting from the extremal boundary.

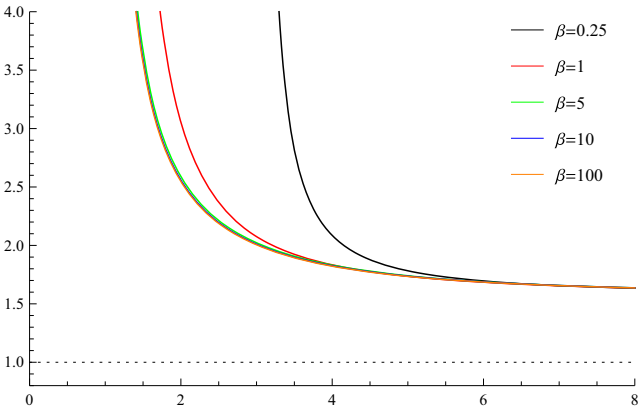


**(b)** Plot of $R_V$ versus $q$ in CV-duality along the $\tilde{\Phi} = 1.5$ curve starting from the extremal boundary.

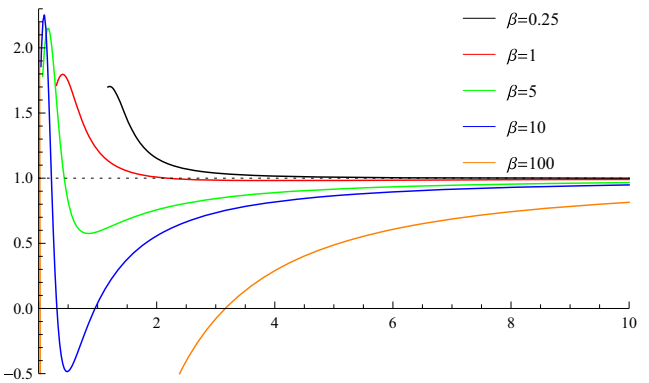


**(c)** Plot of $R_A$ versus $q$ in CA-duality along the $\tilde{\Phi} = 1$ curve starting from the red boundary.

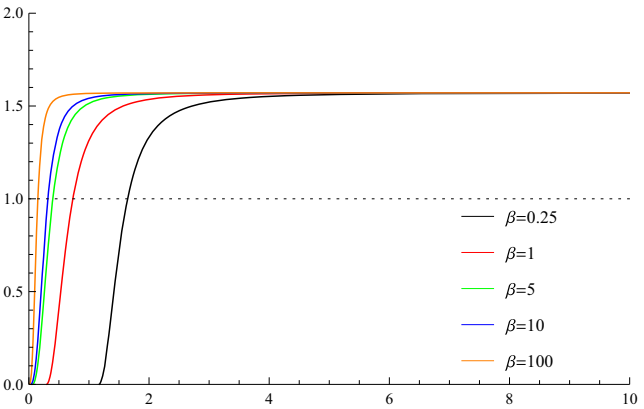


**(d)** Plot of $R_V$ versus $q$ in CV-duality along the $\tilde{\Phi} = 1$ curve starting from the red boundary.

**Fig. 4** The rate of the complexity in CA duality and CV duality divided by the generalized Lloyd bound, $R_A$ and $R_V$ respectively, along the $\tilde{\Phi} = 1$ and $\tilde{\Phi} = 1.5$ curves

In Fig. 4, we plot $R_A$ and $R_V$ along the $\tilde{\Phi} = 1$ and $\tilde{\Phi} = 1.5$ curves for $\beta = 0.25$ (black), $\beta = 1$ (red), $\beta = 5$ (green), $\beta = 10$ (blue), and $\beta = 100$ (orange). As shown in Fig. 4, the $R_A$ curves approach $R_A = 1$ asymptotically from below for large $q$, while the $R_V$ curves approach $R_A = \pi/2$ asymptotically, which agrees with Eqs. (47) and (49). Near extremality, $R_A$ and $R_V$ on the $\tilde{\Phi} = 1.5$ curve go to infinity as predicted by Eqs. (32) and (35). When approaching the red boundary along the $\tilde{\Phi} = 1$ curve, $R_A$ and $R_V$ go above $R_A = 1$ and to zero, respectively, which also agrees with Eqs. (42) and (43).

Along the $\tilde{\Phi} = 1.5$ curve, Fig. 4a shows that the generalized Lloyd bound is satisfied in CA duality for large enough $q$, while Fig. 4b shows that the generalized Lloyd bound is violated in CV duality. Note that the kinks in the $R_A$ curves in Fig. 4a are where the $\tilde{\Phi} = 1.5$ curve enter the "Single Horizon" region from the "Two Horizons" region. Along the $\tilde{\Phi} = 1$ curve, Fig. 4d shows that the generalized Lloyd bound is only satisfied in CV duality for small $q$. It is interesting to see that the $R_A$ curves in Fig. 4c start to oscillate for small $q$ when $\beta$ is large enough ($\beta = 5$, 10, and 100). Even for $\beta = 10$ and 100, there is a range of $q$ over which $\dot{\mathcal{C}}_A < 0$.

In summary, the generalized Lloyd bound is violated in CA duality as we approach the ground states, but this bound tend to be saturated as we go away from the ground states with fixed potential. As noted in [11], the violations near the ground states have something to do with hair. In CV duality, the generalized Lloyd bound is violated everywhere along the constant potential curves, except near the ground states on the red line.

**Table 1** Check of whether the generalized Lloyd bound is violated or satisfied

| | Near extremal line | Near red line | Large $q$ on constant $\Phi$ curve |
|---|---|---|---|
| CA duality | Violated | Violated | Tend to be saturated |
| CV duality | Violated | Satisfied | Violated |

## 4 Discussion and conclusion

In this paper, we first obtained the phase diagram of Born–Infeld AdS black holes and then checked whether the generalized Lloyd bound was violated in CA and CV dualities. In Sect. 2, we showed that the Born–Infeld black hole solution could possess a naked singularity, a single horizon, or two horizons, depending on the values of its parameters $q$ and $m$. Except the $k = 1$ and $d = 3$ case, the boundaries between "Black Hole" region and "No Black Hole" region were extremal lines (blue lines in Fig. 2). However, in the $k = 1$ and $d = 3$ case, there was an additional boundary (red line in Fig. 2a), on which was some regular spacetime with nonvanishing charges. It is noteworthy that unlike a RN AdS black hole, the ground state of a Born–Infeld AdS black hole with potential $\Phi > 0$ could not be the empty AdS spacetime.

In Sect. 3, we calculated the generalized Lloyd bound and the rate of the complexity at late times in CA and CV dualities near the boundaries and for large $q$ on the constant $\Phi$ curves. The results of whether the generalized Lloyd bound was violated are summarized in Table 1. We also found that, for a general static charged AdS black hole with the charge $Q$ near extremality, the generalized Lloyd bound in Eq. (26) was always $\mathcal{O}\left(\delta Q^2\right)$, where $\delta Q \equiv Q - Q_e$, and $Q_e$ was the charge of the extremal black hole with the same potential. If the difference between the outer and inner horizon radii is $\mathcal{O}(\delta Q)$, which is the case for RN AdS and Born–Infeld AdS black holes, then the generalized Lloyd bound is usually violated near extremality.

In the $d = 3$ and $k = 1$ case, we plotted the rate of the complexity in CA and CV dualities divided by the generalized Lloyd bound along the $\tilde{\Phi} = 1$ and $\tilde{\Phi} = 1.5$ curves in Fig. 4. It appears that the generalized Lloyd bound in CA duality was violated near the ground states but tended to be saturated as moving away from the ground states along the constant $\Phi$ curves. On the other hand, the generalized Lloyd bound in CV duality was violated along the constant $\Phi$ curves, except near the ground states on the red line. Since the hair may play a role in the violations near the ground states, it seems from these observations that CA duality is slightly favored.

In this paper, we have focused on the generalized Lloyd bound. However, the Lloyd bound in Eq. (3) is solider than the generalized Lloyd bound in Eq. (4) in quantum information theory, so the violation of the Lloyd bound is a more serious problem for the holographic conjectures of complexity. So we now check whether the Lloyd bound is satisfied for the Born–Infeld AdS black holes. In CA duality, we check the Lloyd bound in the following cases:

1. Single Horizon: It is easy to see from Eq. (22) that the Lloyd bound is always satisfied in this case since $Q\Phi_+$ and $A\,(q)$ are greater than zero.
2. Two Horizons: The results depend on the scalar curvature of the horizon:
   (a) $k = 1$ and 0: We believe that the Lloyd bound is satisfied in these cases. However, it is difficulty to prove it analytically. Instead, we check it numerically. To do that, we define
   $$\tilde{R}_A = \dot{\mathcal{C}}_A / \frac{2M}{\pi\hbar}, \tag{52}$$
   and plot $\tilde{R}_A$ in Fig. 5a in the two cases of $d = 3$, $\beta = 10$ and $L = 1$ for $(q, k) = (0.3, 1)$ and $(q, k) = (0.7, 0)$. Figure 5a shows that the Lloyd bound is satisfied in these two cases.
   (b) $k = -1$: In this case, the Born–Infeld AdS black holes could exist when $m < 0$. In Fig. 2b, we plot the phase diagram for $d = 3$, $\beta = 10$, $L = 1$ and $k = -1$. It shows that the case of two horizons could have $m < 0$, which clearly violate the Lloyd bound since $\dot{\mathcal{C}}_A \geq 0$. Therefore, the Lloyd bound is violated in the region of $m < 0$ and its some neighborhood in the phase diagram. In Fig. 5b, we plot $\tilde{R}_A$ for $q = 0.3$, $d = 3, \beta = 10, L = 1$ and $k = -1$ to show this point. On the other hand, the Lloyd bound is satisfied in the region far enough from $m = 0$. We also plot $\tilde{R}_A$ for $q = 1, d = 3, \beta = 10, L = 1$ and $k = -1$ in Fig. 5a.

In CV duality, we numerically check the Lloyd bound in the following cases:

1. $k = 1$ and 0: We define
   $$\tilde{R}_V = \dot{\mathcal{C}}_V / \frac{2M}{\pi\hbar}, \tag{53}$$
   and plot $\tilde{R}_V$ in Fig. 6a in the cases of $d = 3$, $\beta = 10$ and $L = 1$ for $(q, k) = (0.3, 1)$ and $(q, k) = (0.7, 0)$. It shows that, for large enough $m$, the Lloyd bound is always violated.
2. $k = -1$: The function $\tilde{R}_V$ is plotted in Fig. 6a for $q = 1$, $d = 3, \beta = 10, L = 1$ and $k = -1$. For fixed $q$, it shows

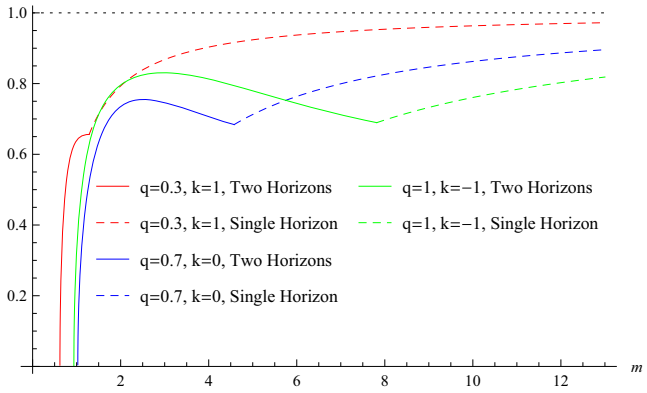


**(a)** Extremal black holes have $m > 0$.

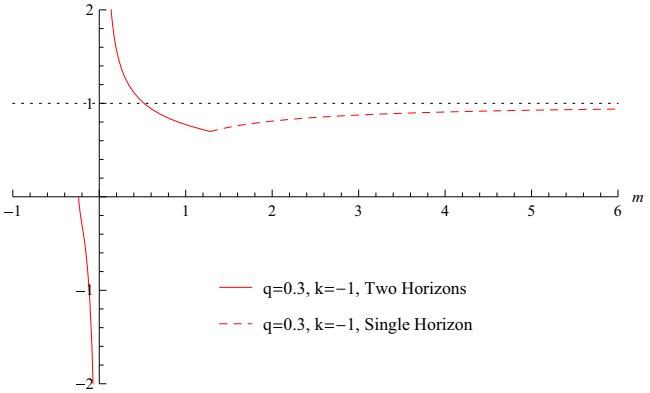


**(b)** Extremal black holes have $m < 0$.

**Fig. 5** The rate of the complexity in CA duality divided by the Lloyd bound, $\tilde{R}_A$. Here we take $d = 3$, $L = 1$ and $\beta = 10$

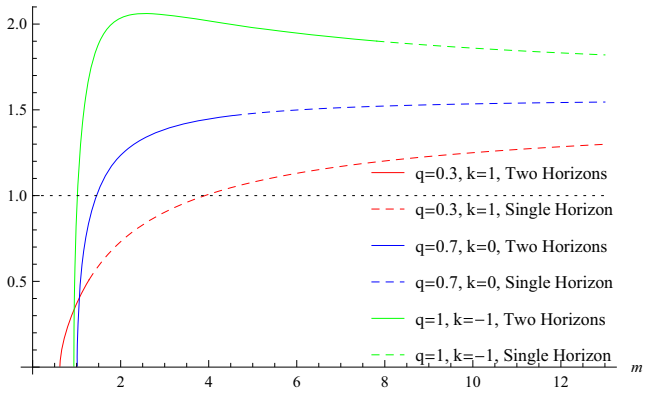


**(a)** Extremal black holes have $m > 0$.

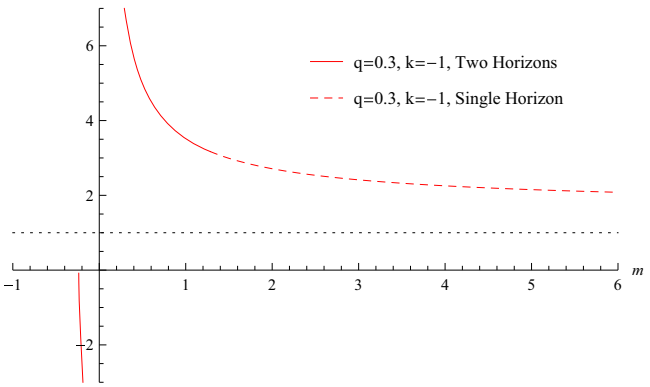


**(b)** Extremal black holes have $m < 0$.

**Fig. 6** The rate of the complexity in CV duality divided by the Lloyd bound, $\tilde{R}_V$. Here we take $d = 3$, $L = 1$ and $\beta = 10$

that if an extremal black hole has $m > 0$, the Lloyd bound is satisfied for the black holes with small enough $m$ but violated for these with large enough $m$. We plot $\tilde{R}_A$ for $q = 0.3$, $d = 3$, $\beta = 10$, $L = 1$ and $k = -1$ in Fig. 6b. If an extremal black hole has $m < 0$, the Lloyd bound is violated for all or most of the black holes with the same charge as that of the extremal black hole.

On the quantum information theory side, researchers generally believe that the linear growth of the complexity at late time and the (generalized) Lloyd bound are true but have difficulty to prove them. The first conjecture has motivated several proposals of a holographic dual to the complexity. In these proposals, satisfying the (generalized) Lloyd bound on the gravity side could provide strong evidence for these dualities. However, it is not uncommon to encounter the violations of the (generalized) Lloyd bound, which might imply that:

- Something is wrong with the holographic duality.
- Calculations on the gravity side cannot be trusted. For a general static charged AdS black hole near extremality, we found that the generalized Lloyd bound was always badly violated. This violation can be explained by the existence of the hair [11], which make the calculations unreliable when its effect is important. When a black hole is far away from the ground state, one expects that the hair plays a much less important role, and hence the calculation can be trusted. We found that in CA duality, when a Born–Infeld AdS black hole moved along a constant potential curve far enough away from the ground state, it always satisfied and tended to saturate the generalized Lloyd bound. One the other hand, the generalized Lloyd bound was always violated in CV duality in this case, which requires something else to explain the violation. We also found that, for a Born–Infeld AdS black hole with $m < 0$, the Lloyd bound was always violated. In this case, the black hole has negative ADM mass, and

hence one should check whether this black hole solution has any pathological properties, which is out of the scope of this paper.

- One might need alter the bound by a pre-factor [20]. As noted in [20], the (generalized) Lloyd bound should only be trusted up to an overall factor. In this case, the (generalized) Lloyd bound can be changed to

$$\dot{\mathcal{C}} \leq \frac{\alpha}{\pi\hbar} M \quad \text{and} \quad \dot{\mathcal{C}} \leq \frac{\alpha}{\pi\hbar}\left[(M - Q\Phi) - (M - Q\Phi)_{\text{gs}}\right], \tag{54}$$

respectively, where $\alpha$ is some number. In CV duality, we found that, for a Born–Infeld AdS black hole on a constant potential curve far enough away from the ground state, $\dot{\mathcal{C}}$ was $\pi/2$ times as large as the generalized Lloyd bound. Similarly, we also found that $\dot{\mathcal{C}}$ was $\pi/2$ times as large as the Lloyd bound for a black hole with large enough mass. It seems that $\alpha = \pi$ would place CV duality in a much better position.

Finally, we want to briefly discuss the differences between our results and these of RN AdS black holes. The ground state of a RN AdS black hole is either the empty AdS space or some extremal black hole. However, the ground state of a Born–Infeld AdS black hole is either some charged regular spacetime or extremal black hole, but could not be the empty AdS space as long as the potential is not zero. As shown by Eq. (5.15) in [20] and Fig. 6 in [11], if the ground state was the empty AdS space, $\dot{\mathcal{C}}_A$ for a RN AdS black hole with $d = 3$ and $k = 1$ always violated the generalized Lloyd bound along a constant potential curve, even when $q \to \infty$. However, for a Born–Infeld AdS black hole, our results show that the generalized Lloyd bound in CA duality is satisfied for large enough $q$ along a constant potential curve. When $q$ is very large with fixed potential, we have obtained $\frac{q}{r_+^{d-1}} \ll 1$, and the metric in Eq. (7) is almost the same as that of a RN AdS black hole outside the outer horizon. In this case, physics over the region outside the outer horizon of the Born–Infeld AdS black hole does not differ much from that of the RN AdS black hole. A different behavior of $\dot{\mathcal{C}}_A$ for RN AdS and Born–Infeld AdS black holes with large $q$ on the constant potential curves means that the complexity encodes physics behind black hole horizons.

**Acknowledgements** We are grateful to Song He, Houwen Wu, and Zheng Sun for useful discussions. This work is supported in part by NSFC (Grant nos. 11005016, 11175039 and 11375121).



## Appendix A: Rate of action of Born–Infeld AdS black holes

In this appendix, we use the methods in [12] to calculate the change of action, $\delta S = S(t_0 + \delta t) - S(t_0)$, of the Wheeler–deWitt patch at late times. The Penrose diagrams for two-sided eternal Born–Infeld AdS black holes are illustrated in Fig. 7, along with the Wheeler–deWitt patches at $t = t_0$ and $t_0 + \delta t$. Here we fix the time on the right boundary and only vary it on the left boundary. There is a divergence appearing when calculating the action near the boundary $r = \infty$. So a surface of constant $r = r_{\max}$ is defined to regulate the action. In [24], the action was regulated by defining the boundaries of the WdW patch originate slightly inside the AdS boundary. It turns out that these two choices for the regulator yield the same results. We also introduce a spacelike surface $r = \varepsilon$ near the future singularities and let $\varepsilon \to 0$ at the end of calculations. Note that we have an affine parametrization for each null surface, and these make no contribution to the action. To calculate $\delta S$, we introduce the null coordinates $u$ and $v$ in the metric (7):

$$\begin{aligned} u &= t - r^* \\ v &= t + r^*, \end{aligned} \tag{A1}$$

where

$$r^* = \int f^{-1}(r)\, \mathrm{d}r. \tag{A2}$$

1. Single horizon case

We calculate $\delta S$ for a Born–Infeld AdS black hole with a single horizon, whose Penrose diagram is illustrated in Fig. 7a. Due to time translation, the joint contributions from $\mathcal{D}$ and $\mathcal{D}'$ are identical, and they therefore make no contribution to $\delta S$. Similarly, the joint and surface contributions from $\mathcal{MN}$ cancel against those from $\mathcal{M}'\mathcal{N}'$ on $r = r_{\max}$ in calculating $\delta S$. Therefore, we have

$$\begin{aligned} \delta S = {} & S_{\mathcal{V}_1} - S_{\mathcal{V}_2} + 2\int_{\mathcal{S}} d^d x \sqrt{|h|} K \\ & + 2\int_{\mathcal{B}'} d^{d-1} x \sqrt{\sigma} a - 2\int_{\mathcal{B}} d^{d-1} x \sqrt{\sigma} a, \end{aligned} \tag{A3}$$

where we follow the conventions in [13].

Using the Born–Infeld AdS black hole solution (7), we find that the volume contribution is

$$S_{\mathcal{V}} = \Omega_{k,d-1} \int_{\mathcal{V}} \mathrm{d}\omega F(r), \tag{A4}$$

where $\omega = \{u, v\}$, and

$$F(r) = 2r^{d-2}\left(k - \frac{m}{r^{d-2}} - f(r)\right). \tag{A5}$$

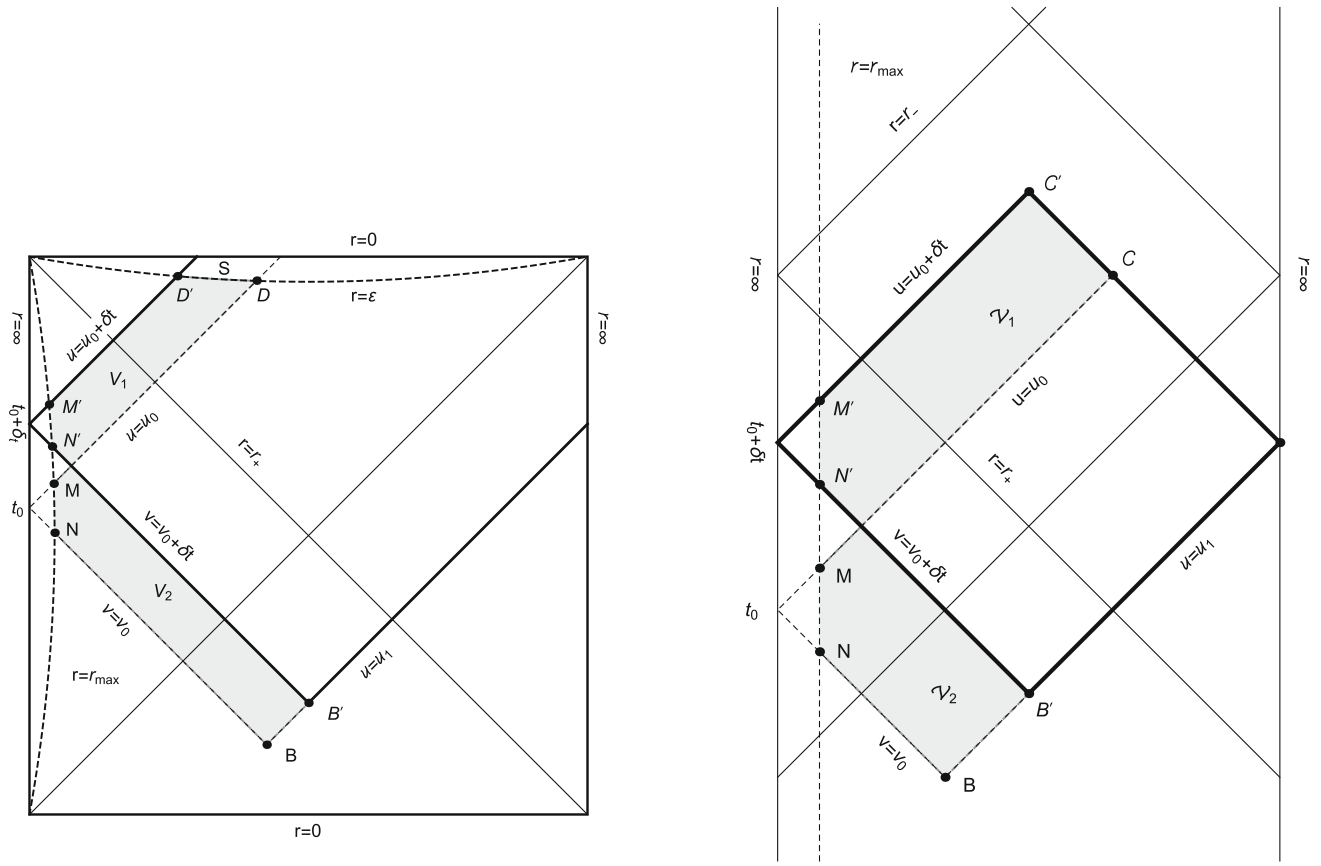


**(a)** Single Horizon Case **(b)** Two Horizons Case

**Fig. 7** Wheeler–deWitt patches of Born–Infeld AdS black holes at $t_L = t_0$ and $t_L = t_0 + \delta t$. The lines $r = r_{\max}$ and $r = \varepsilon$ are cut-off surfaces

The region $\mathcal{V}_1$ is bounded by the null surfaces $u = u_0$, $u = u_0 + \delta t$, $v = v_0 + \delta t$, the spacelike surface $r = \varepsilon$, and the timelike surface $r = r_{\max}$. Using Eq. (A4), we have

$$S_{\mathcal{V}_1} = \Omega_{k,d-1} \int_{u_0}^{u_0+\delta t} \mathrm{d}u F(r)\,|_{\varepsilon}^{\min\{r_{\max},\rho(u)\}} \mathrm{d}r, \tag{A6}$$

where $r^*(\rho(u)) = (v_0 + \delta t - u)/2$. Since $\lim_{r\to 0} F(r) = -2A(q)$, we find that

$$S_{\mathcal{V}_1} = \Omega_{k,d-1} \int_{u_0}^{u_0+\delta t} \mathrm{d}u \left[F(r)\,|_{r=\min\{r_{\max},\rho(u)\}} + 2A(q)\right], \tag{A7}$$

where $A(q)$ is given by Eq. (15). Similarly for $\mathcal{V}_2$, one has

$$S_{\mathcal{V}2} = \Omega_{k,d-1} \int_{v_0}^{v_0+\delta t} \mathrm{d}v F(r)\,|_{\rho_1(v)}^{\min\{r_{\max},\rho_0(v)\}}, \tag{A8}$$

where $r^*\left(\rho_{0/1}(v)\right) = \left(v - u_{0/1}\right)/2$. Performing the change of variables $u = u_0 + v_0 + \delta t - v$, we have

$$\int_{v_0}^{v_0+\delta t} \mathrm{d}v F(r)\,|_{r=\min\{r_{\max},\rho_0(v)\}} = \int_{u_0}^{u_0+\delta t} \mathrm{d}u F(r)\,|_{r=\min\{r_{\max},\rho(u)\}}, \tag{A9}$$

and hence

$$S_{\mathcal{V}_1} - S_{\mathcal{V}_2} = \Omega_{k,d-1} \left[\int_{v_0}^{v_0+\delta t} \mathrm{d}v F(r)\,|_{r=\rho_1(v)} + 2A(q) \int_{u_0}^{u_0+\delta t} \mathrm{d}u\right]. \tag{A10}$$

At late times, one has $\rho_1(v) \approx r_+$, and

$$S_{\mathcal{V}_1} - S_{\mathcal{V}_2} = \Omega_{k,d-1} \left[F(r_h) + 2A(q)\right] \delta t. \tag{A11}$$

There is a timelike hypersurface at $r = \varepsilon$, with outward-directed normal vectors from the region of interest. The normal vector is

$$n_\mu \mathrm{d}x^\mu = \frac{-1}{\sqrt{-f(r)}} \mathrm{d}r. \tag{A12}$$

The trace of extrinsic curvature is

$$K = \frac{1}{r^{d-1}}\partial_r\left(r^{d-1}\sqrt{-f\left(r\right)}\right). \tag{A13}$$

Therefore, the surface contributions from $r = \varepsilon$ is

$$\begin{aligned} &2\int_{\mathcal{S}} d^dx\sqrt{|h|}K \\ &= 2\left(m - A\left(q\right)\right)\Omega_{k,d-1}\frac{\delta t}{r^{d/2-1}}\partial_r\left(r^{d/2}\right)|_{r=\varepsilon} \\ &= \left[m - A\left(q\right)\right]\mathrm{d}\Omega_{k,d-1}\delta t, \end{aligned} \tag{A14}$$

where we use $\sqrt{|h|} = \sqrt{-f\left(r\right)}r^{d-1}\mathrm{d}\Omega_{k,d-1}$.

Following [13], the integrand $a$ in the joint terms of Eq. (A3) is

$$\begin{aligned} a &= \epsilon\ln\left|\mathbf{k}_1\cdot\mathbf{k}_2/2\right|, \\ \epsilon &= -\mathrm{sign}\left(\mathbf{k}_1\cdot\mathbf{k}_2\right)\mathrm{sign}\left(\hat{\mathbf{k}}\cdot\mathbf{k}_2\right), \end{aligned} \tag{A15}$$

where for $\mathcal{B}$ and $\mathcal{B}'$,

$$\begin{aligned} \left(\mathbf{k}_1\right)_\mu &= -c_1\partial_\mu\left(t + r^*\right), \\ \left(\mathbf{k}_2\right)_\mu &= c_2\partial_\mu\left(t - r^*\right), \end{aligned} \tag{A16}$$

and the auxiliary null vectors $\hat{\mathbf{k}}$ is the null vector orthogonal to the joint and pointing outward from the boundary region. Therefore, we find that

$$\begin{aligned} &2\int_{\mathcal{B}'} d^{d-1}x\sqrt{\sigma}a - 2\int_{\mathcal{B}} d^{d-1}x\sqrt{\sigma}a \\ &= 2\Omega_{k,d-1}\left[h\left(r_{\mathcal{B}'}\right) - h\left(r_{\mathcal{B}}\right)\right], \end{aligned} \tag{A17}$$

where

$$h\left(r\right) = r^{d-1}\ln\left(-\frac{f\left(r\right)}{c_1c_2}\right). \tag{A18}$$

At late times, we have $r_{\mathcal{B}} \approx r_+$ and

$$\begin{aligned} h\left(r_{B'}\right) - h\left(r_B\right) &= \frac{f\left(r\right)}{2}\frac{\mathrm{d}h\left(r\right)}{\mathrm{d}r}|_{r=r_B}\delta t \\ &= \frac{1}{2}r^{d-1}\frac{\mathrm{d}f\left(r\right)}{\mathrm{d}r}|_{r=r_+}\delta t, \end{aligned} \tag{A19}$$

where we use $\mathrm{d}r = f\left(r\right)\delta t/2$ on $u = u_1$. Thus, this gives

$$\begin{aligned} &2\int_{\mathcal{B}'} d^{d-1}x\sqrt{\sigma}a - 2\int_{\mathcal{B}} d^{d-1}x\sqrt{\sigma}a \\ &= \Omega_{k,d-1}r_+^{d-1}f'\left(r_+\right)\delta t. \end{aligned} \tag{A20}$$

Combining Eqs. (A10), (A14), and (A20), we arrive at

$$\frac{\mathrm{d}S}{\mathrm{d}t} = 2M - Q\Phi_+ - \left(d-2\right)A\left(q\right)\Omega_{k,d-1} \tag{A21}$$

where we use $f\left(r_+\right) = 0$, and $\Phi_+$ is the potential $\Phi$ evaluated at $r = r_+$. When $k = 1$ and $d = 3$, Eq. (A21) becomes

$$\frac{\mathrm{d}S}{\mathrm{d}t} = 2M - Q\Phi_+ - 16\pi\beta^{1/2}Q^{3/2}\frac{\Gamma\left(1/4\right)\Gamma\left(5/4\right)}{3\Gamma\left(1/2\right)}, \tag{A22}$$

where $Q = q$ in the $k = 1$ and $d = 3$ case. Taking into account that $16\pi G = 1$ in our paper and $G = 1$ in [24], our result ( A22) agrees with Eq. (3.26) in [24].

2. The case of two horizons

The Penrose diagram for a Born–Infeld AdS black hole with two horizons is illustrated in Fig. 7b. Thus, we have

$$\begin{aligned} \delta S = S_{\mathcal{V}_1} - S_{\mathcal{V}_2} &+ 2\int_{\mathcal{B}'} d^{d-1}x\sqrt{\sigma}a - 2\int_{\mathcal{B}} d^{d-1}x\sqrt{\sigma}a \\ &+2\int_{\mathcal{C}'} d^{d-1}x\sqrt{\sigma}a - 2\int_{\mathcal{C}} d^{d-1}x\sqrt{\sigma}a. \end{aligned} \tag{A23}$$

While the volume contribution $S_{\mathcal{V}_2}$ is also given by Eq. (A8), we find that, in this case,

$$S_{\mathcal{V}_1} = \Omega_{k,d-1}\int_{u_0}^{u_0+\delta t}\mathrm{d}u\,F\left(r\right)|_{\tilde{\rho}_1(u)}^{\min\{r_{\max},\rho(u)\}}\mathrm{d}r, \tag{A24}$$

where

$$r^*\left(\tilde{\rho}_1\left(u\right)\right) = \frac{v_1 - u}{2}. \tag{A25}$$

Hence the volume contribution to $\delta S$ is

$$\begin{aligned} S_{\mathcal{V}_1} - S_{\mathcal{V}_2} &= \Omega_{k,d-1}\left[\int_{v_0}^{v_0+\delta t}\mathrm{d}v\,F\left(r\right)|_{r=\rho_1(v)}\right. \\ &\quad\left. - \int_{u_0}^{u_0+\delta t}\mathrm{d}u\,F\left(r\right)|_{r=\tilde{\rho}_1(u)}\mathrm{d}r\right] \\ &= \Omega_{k,d-1}\left[F\left(r_+\right) - F\left(r_-\right)\right]\delta t, \end{aligned} \tag{A26}$$

where the portion of $\mathcal{V}_1$ below the future horizon cancels against the portion of $\mathcal{V}_2$ above the past horizon. The joint contributions from $\mathcal{B}$ and $\mathcal{B}'$ are the same as in the case with a single horizon. Analogously to calculating the joint contributions from $\mathcal{B}$ and $\mathcal{B}'$, we find that

$$\begin{aligned} &2\int_{\mathcal{C}'} d^{d-1}x\sqrt{\sigma}a - 2\int_{\mathcal{C}} d^{d-1}x\sqrt{\sigma}a \\ &= -\Omega_{k,d-1}r_-^{d-1}f'\left(r_-\right)\delta t, \end{aligned} \tag{A27}$$

where $r_-$ is the inner horizon radius. Summing up all the contributions, we obtain

$$\frac{\mathrm{d}S}{\mathrm{d}t} = Q\Phi_- - Q\Phi_+, \tag{A28}$$

where $\Phi_\pm$ is the potential $\Phi$ evaluated at $r = r_\pm$. When approaching the boundary between the "Single Horizon" and "Two Horizons" regions, we have $r_- \to 0$ and $Q\Phi_- \to$

$A(q)\,\mathrm{d}\Omega_{k,d-1}$. Since $m = A(q)$ on this boundary, Eq. (A28) becomes

$$\frac{\mathrm{d}S}{\mathrm{d}t} \to 2M - Q\Phi_+ - (d-2)\,A(q)\,\Omega_{k,d-1}. \tag{A29}$$

Comparing with Eq. (A21), we find that $\mathrm{d}S/\mathrm{d}t$ is continuous when crossing this boundary.

## References


1. S. Ryu, T. Takayanagi, Holographic derivation of entanglement entropy from AdS/CFT. Phys. Rev. Lett. **96**, 181602 (2006). https://doi.org/10.1103/PhysRevLett.96.181602. arXiv:hep-th/0603001
2. S. Ryu, T. Takayanagi, Aspects of holographic entanglement entropy. JHEP **0608**, 045 (2006). https://doi.org/10.1088/1126-6708/2006/08/045. arXiv:hep-th/0605073
3. L. Susskind, Computational complexity and black hole horizons. Fortsch. Phys. **64**, 24 (2016). https://doi.org/10.1002/prop.201500092. arXiv:1403.5695 [hep-th], arXiv:1402.5674 [hep-th]
4. D. Stanford, L. Susskind, Complexity and Shock Wave Geometries. Phys. Rev. D **90**(12), 126007 (2014). https://doi.org/10.1103/PhysRevD.90.126007. arXiv:1406.2678 [hep-th]
5. L. Susskind, Y. Zhao, Switchbacks and the bridge to nowhere. arXiv:1408.2823 [hep-th]
6. L. Susskind, Entanglement is not enough. Fortsch. Phys. **64**, 49 (2016). https://doi.org/10.1002/prop.201500095. arXiv:1411.0690 [hep-th]
7. J. Watrous, "Quantum computational complexity," in Encyclopedia of Complexity and Systems Science, ed., R. A. Meyers (2009) 7174–7201. arXiv:0804.3401 [quant-ph]
8. S. Gharibian, Y. Huang, Z. Landau, S.W. Shin, Quantum hamiltonian complexity. Found. Trends Theoret. Comput. Sci. **10**, 159–282 (2015). arXiv:1401.3916 [quant-ph]
9. T.J. Osborne, Hamiltonian complexity. Rep. Progress Phys. **75**, 022001 (2012). arXiv:1106.5875 [quant-ph]
10. A.R. Brown, D.A. Roberts, L. Susskind, B. Swingle, Y. Zhao, Holographic complexity equals bulk action?, Phys. Rev. Lett. **116**(19), 191301 (2016). https://doi.org/10.1103/PhysRevLett.116.191301. arXiv:1509.07876 [hep-th]
11. A.R. Brown, D.A. Roberts, L. Susskind, B. Swingle, Y. Zhao, Complexity, action, and black holes, Phys. Rev. D **93**(8), 086006 (2016). https://doi.org/10.1103/PhysRevD.93.086006. arXiv:1512.04993 [hep-th]
12. L. Lehner, R.C. Myers, E. Poisson, R.D. Sorkin, Gravitational action with null boundaries, Phys. Rev. D **94**(8), 084046 (2016). https://doi.org/10.1103/PhysRevD.94.084046. arXiv:1609.00207 [hep-th]
13. D. Carmi, R.C. Myers, P. Rath, Comments on holographic complexity. arXiv:1612.00433 [hep-th]
14. A. Reynolds, S.F. Ross, Divergences in holographic complexity. arXiv:1612.05439 [hep-th]
15. K.Y. Kim, C.Niu, R.Q. Yang, Surface counterterms and regularized holographic complexity. arXiv:1701.03706 [hep-th]
16. S. Chapman, H. Marrochio, R.C. Myers, Complexity of Formation in Holography, JHEP **1701**, 062 (2017). https://doi.org/10.1007/JHEP01(2017)062. arXiv:1610.08063 [hep-th]
17. S. Lloyd, Ultimate physical limits to computation, Nature **406**(6799), 1047–1054 (2000)
18. R.Q. Yang, Strong energy condition and complexity growth bound in holography, Phys. Rev. D **95**(8), 086017 (2017). https://doi.org/10.1103/PhysRevD.95.086017. arXiv:1610.05090 [gr-qc]
19. R.G. Cai, S.M. Ruan, S.. Wang, R.Q. Yang, R.H. Peng, Action growth for AdS black holes, JHEP **1609**, 161 (2016). https://doi.org/10.1007/JHEP09(2016)161. arXiv:1606.08307 [gr-qc]
20. J. Couch, W. Fischler, P.H. Nguyen, Noether charge, black hole volume, and complexity. arXiv:1610.02038 [hep-th]
21. W.J. Pan, Y.C. Huang, Holographic complexity and action growth in massive gravities. arXiv:1612.03627 [hep-th]
22. M. Alishahiha, A. Faraji Astaneh, A. Naseh, M.H. Vahidinia, On complexity for higher derivative gravities. arXiv:1702.06796 [hep-th]
23. H. Huang, X.H. Feng, H. Lu, Holographic complexity and two identities of action growth. arXiv:1611.02321 [hep-th]
24. R.G. Cai, M. Sasaki, S.J. Wang, Action growth of charged black holes with a single horizon. arXiv:1702.06766 [gr-qc]
25. T.K. Dey, Born–Infeld black holes in the presence of a cosmological constant, Phys. Lett. B **595**, 484 (2004). https://doi.org/10.1016/j.physletb.2004.06.047 [hep-th/0406169]
26. R.G. Cai, D.W. Pang, A. Wang, Born–Infeld black holes in (A)dS spaces, Phys. Rev. D **70**, 124034 (2004). https://doi.org/10.1103/PhysRevD.70.124034 [hep-th/0410158]